Correspondence

Electrostatic Transducers for Micromechanical Resonators: Free Space and Solid Dielectric

Ville Kaajakari, *Member, IEEE*, Ari T. Alastalo, and Tomi Mattila, *Member, IEEE*

***Abstract*—Three electrostatic transduction methods are analyzed for a micromechanical, longitudinal mode, beam resonator. The conventional parallel plate transducer placed at the location of maximum displacement is compared to two solid, dielectric transducers internal to the resonator. Although the solid dielectric offers higher permittivity than the free-space-filled transducers, the unfavorable locations of the internal transducers reduce or even remove the performance advantage of the higher permittivity.**

I. Introduction

Micromechanical resonators have been demonstrated to offer high quality factors, $Q > 100,000$ at 10 MHz [1] and $Q > 1,000$ at 1 GHz [2], comparable to those of macroscopic resonators such as quartz crystals and surface acoustic wave (SAW) resonators, and are, therefore, a potential alternative to the size-consuming, off-chip filters and oscillators. Electrostatic coupling to microresonators has been of considerable interest due to the compatibility with integrated circuit fabrication processes because no special materials, such as piezoelectrics, are required. Unfortunately, the electrostatic coupling is rather ineffective for high-frequency resonators. As a result, the typical resonator impedances are impractically high (over 100 kΩ at gigahertz frequencies). In order to obtain usable impedance levels, very small electrode gaps (<100 nm) are desired. The lower limit to the gap size is set by fabrication challenges, the minimum resonator vibration amplitude for sufficient energy storage, or nonlinear effects such as intermodulation distortion arising from the inverse relationship between the transducer capacitance and the electrode gap [3].

Usually, the electrode gap has been free space, which offers nearly perfect acoustic isolation due to a large impedance discontinuity. Recently, the use of high permittivity materials have been proposed as a way to enhance the electrostatic coupling [4], [5]. In a typical configuration, filling the electrode gap with a solid material would introduce acoustic losses as the solid material does not provide the ideal impedance mismatch [6]. Nevertheless, improvement in the transducer coupling coefficient can be achieved, at the cost of lowered quality factor. In [7], the introduction of $\epsilon = 7.8\epsilon_0$ dielectric and reduction of the gap size by factor of four, lead to an $8x$ improvement in motional impedance—a significant but small improvement in comparison to $7.8^2 \cdot 4^4 > 10^4 x$ improvement expected for an ideal transducer with no change in the quality factor. As an alternative to the typical configuration, electrostatic transduction using solid dielectric internal to the resonator [4] or on top of the resonator [5] have been proposed.

In this paper, an analytical model for the different transduction methods is developed, and the transducers are compared for a beam resonator. It is found that, as the traditional parallel plate transducer affects the optimal location of the largest resonator displacement, it generates comparatively large force and current. The solid, "internal", transducer placed in the middle of the resonator results in relatively poor performance as the transducer acts in the small displacement region. Transducers placed on top of the resonator act on the entire beam, but because the actuation is based on the Poisson's effect, the transduction efficiency also is decreased.

II. Lumped Model for Forced Vibrations

Fig. 1 shows an infinitesimal beam element with length $\mathrm{d}x$ and cross-sectional area A [9], [10]. The beam can deform without external constraints in z and y directions (stresses $T_z = T_y = 0$). The forces acting on the element are the external excitation force f_e and the stress force $f_T = YA(\partial u/\partial x)$, where u is the material deformation and Y is the Young's modulus. Thus, the Newton's equation of motion for the infinitesimal element is:

$$\rho A \frac{\partial^2 u}{\partial t^2}\mathrm{d}x = f_T|_{x_0+\mathrm{d}x} - f_T|_{x_0} + f_e|_{x_0+\mathrm{d}x} - f_e|_{x_0} = YA\frac{\partial^2 u}{\partial x^2}\mathrm{d}x + \frac{\partial f_e}{\partial x}\mathrm{d}x, \qquad (1)$$

where ρ is the density. Dividing (1) by $\mathrm{d}x$ and including the damping [11] gives the wave equation for the longitudinal beam vibrations[1]:

$$\rho A\frac{\partial^2 u(x,t)}{\partial t^2} - bA\frac{\partial^3 u(x,t)}{\partial t \partial x^2} - YA\frac{\partial^2 u(x,t)}{\partial x^2} = \frac{\partial f_e(x,t)}{\partial x}. \qquad (2)$$

where (2) is the-well known wave equation for longitudinally vibrating beams [9], [10]. The implicit assumption of using Young's modulus in (2) is that the beam is allowed to deform freely in y- and z-directions.

Manuscript received May 5, 2006; accepted July 6, 2006. This work is supported by the Academy of Finland (grant 20542).

The authors are with VTT Technical Research Center of Finland, Tietotie 3, Espoo, FIN-02150, Finland (e-mail: ville@kaajakari.net).

Digital Object Identifier 10.1109/TUFFC.2006.197

[1]This is a one-dimensional (1-D) version of the 3-D wave equation: where $\mathbf{T} = \mathbf{c} : \mathbf{S} + \mathbf{T_e}$ and $\mathbf{T_e}$ is the electric field generated stress (compare to $\mathbf{T} = \mathbf{c} : \mathbf{S} + \mathbf{e} \cdot \mathbf{E}$ for piezoelectric materials) [11].

0885–3010/$20.00 © 2006 IEEE

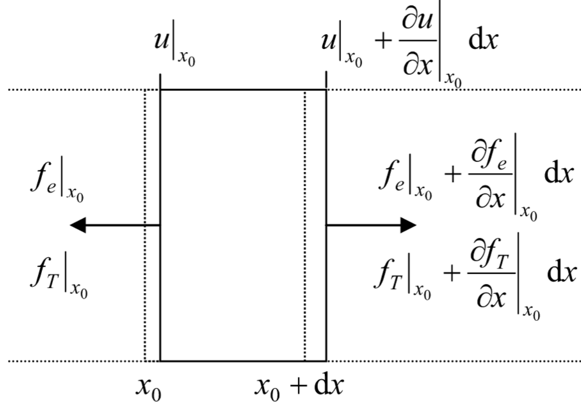

Fig. 1. Diagram showing forces and displacements for an infinitesimal beam element having length dx and cross-sectional area A.

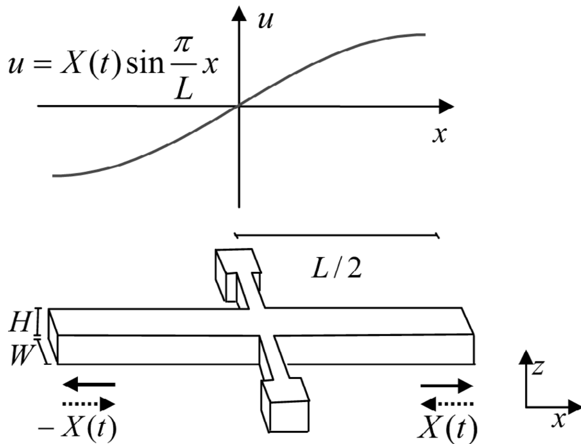

Fig. 2. Longitudinal mode beam resonator [8].

As an example, we consider a beam with a cross-sectional area $A = WH$ and a length L shown in Fig. 2. Assuming that the quality factor Q of the beam resonator is sufficiently large to make the excitation of the higher-order modes negligible, the solution to (2) may be approximated by the first mode:

$$u(x,t) = X(t) \sin kx, \tag{3}$$

where $k = \pi/L$ is the wave number and $X(t)$ is the motion at the beam end. Substituting (3) into (2) gives:

$$\rho A \ddot{X}(t) \sin kx + bAk^2 \dot{X}(t) \sin kx + YAk^2 X(t) \sin kx = \frac{\partial f(x,t)}{\partial x}, \tag{4}$$

where the dot denotes the time derivative. Multiplying (4) with $\sin kx$ and integrating over the beam length leads to:

$$\frac{\rho AL}{2} \ddot{X}(t) + \frac{bALk^2}{2} \dot{X}(t) + \frac{YAk^2 L}{2} X(t) = F(t), \tag{5}$$

where we have defined:

$$F(t) = \int_{-L/2}^{L/2} \frac{\partial f_e(x,t)}{\partial x} \sin kx \, \mathrm{d}x. \tag{6}$$

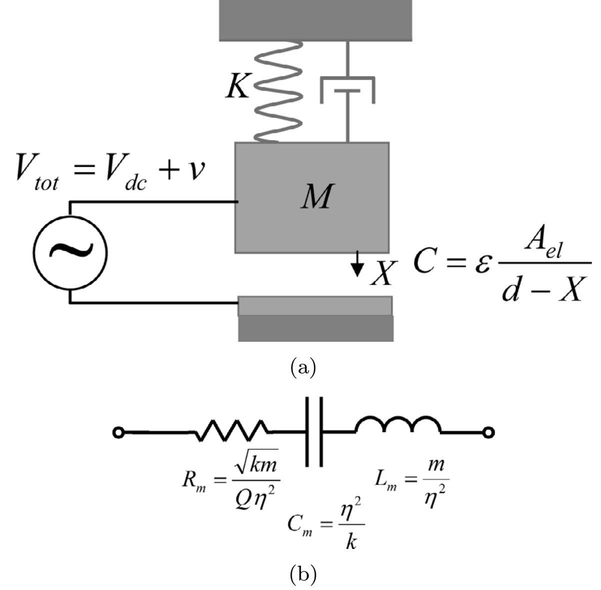

Fig. 3. Lumped mechanical and electrical model for the resonator. (a) Lumped mechanical resonator. (b) Electrical equivalent circuit for the resonator in Fig. 3(a).

Recognizing the effective mass, the damping coefficient, and the spring constant as:

$$\begin{aligned} M &= \rho AL/2, \\ \gamma &= bALk^2/2, \\ K &= YAk^2 L/2 = \pi^2 YA/2L, \end{aligned} \tag{7}$$

leads to:

$$M\ddot{X}(t) + \gamma \dot{X}(t) + KX(t) = F(t). \tag{8}$$

The quality factor is defined as $Q = \sqrt{KM}/\gamma$. Thus, the mechanical resonator properties M, γ, and K do not depend on the transducer force f_e, and only the force F is dependent on transducer location.

III. Electrical Equivalent Circuit

A common scenario for actuation of microresonators is that the transducer is located at the resonator edge, and the motion X directly modulates the parallel electrode capacitance C as illustrated in Fig. 3(a). In this case, the lumped force acting on the resonator can be obtained directly from:

$$F_e = \frac{\partial}{\partial X} \left(\frac{1}{2} C V_{\mathrm{tot}}^2 \right), \tag{9}$$

where $V_{\mathrm{tot}} = V_{\mathrm{dc}} + v(t)$ is the sum of direct current (DC)-bias and alternating current (AC)-voltage $v(t)$ at frequency ω. For small electrode displacements, the time harmonic force at ω is:

$$F_e = \eta v, \tag{10}$$

where the electromechanical transduction factor has been defined as:

$$\eta = \frac{\epsilon_0 A_{\mathrm{el}}}{d^2} V_{\mathrm{dc}}, \tag{11}$$

here ϵ_0 is the permittivity of free space, A_{el} is the total electrode area (for the beam resonator example, $A_{\mathrm{el}} = 2WH$ as the beam is actuated at both ends), and d is the initial electrode gap. The current through the electrode is:

$$i = \frac{\partial (CV_{\mathrm{tot}})}{\partial t} \approx \frac{\partial C}{\partial t} V_{\mathrm{dc}} + C_0 \frac{\partial v}{\partial v} = \eta \dot{X} + C_0 \dot{v}. \tag{12}$$

The second term is recognized as the normal AC-current through the capacitor, and the first term is the motional current $i_m = \eta \dot{X}$ due to the time-varying capacitance.

By combining (8), (10), and (12), an electrical equivalent for the resonator shown in Fig. 3(b) can be derived. Here, the circuit parameters are:

$$\begin{aligned} R_m &= \gamma/\eta^2 = \sqrt{KM}/Q\eta^2, \\ C_m &= \eta^2/K, \text{ and} \\ L_m &= M/\eta^2. \end{aligned} \tag{13}$$

The important observation is that, to obtain a small motional resistance R_m, a large electromechanical transduction factor η is needed. In the following section, the transduction factor is evaluated using the wave equation approach for three different capacitive coupling methods.

IV. Electrostatic Coupling Coefficients

Fig. 4 shows three different electrode configurations. The conventional parallel plate transducer in Fig. 4(a) has the actuating electrodes located at the beam ends. The "internal transducer" in Fig. 4(b) is located in the beam center and is filled with a solid dielectric material. The "Poisson's effect transducer" in Fig. 4(c) has the solid transducer on top of the beam. In this section, the three transducers are compared in terms of electromechanical coupling coefficients.

A. Parallel Plate Transducer

The electromechanical transduction for the parallel plate transducer was derived using the lumped model in Section III. In order to introduce the distributed wave formalism required to account for the transducer location, the beam in Fig. 4(a) is considered. The electromechanical coupling to the beam is done by the two parallel plate transducers with area WH, gap d, permittivity ϵ_p, and bias voltage V_{dc} at the beam ends. Considering an infinitesimal beam element at the right beam end, the force on the right side is:

$$f_e|_{\frac{L}{2}} = \frac{\partial C}{\partial x} V_{\mathrm{dc}} v = \frac{\epsilon_p WH}{d^2} V_{\mathrm{dc}} v, \tag{14}$$

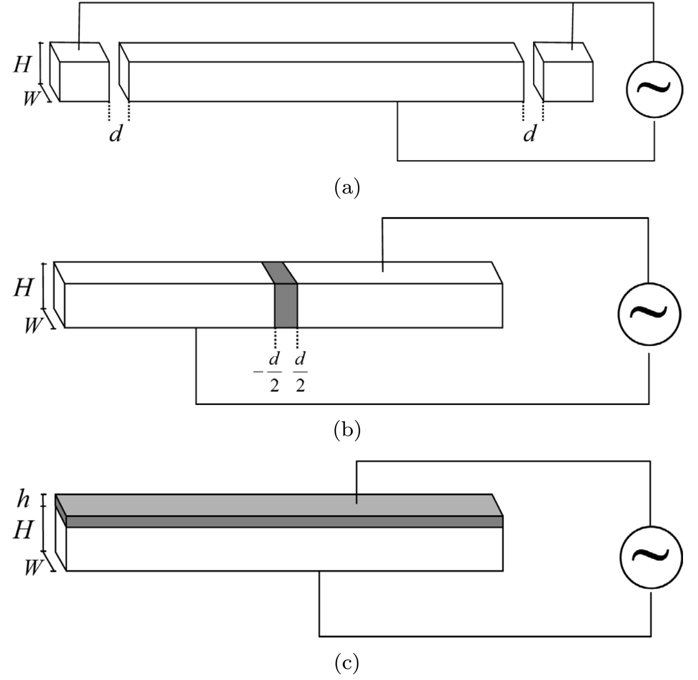

Fig. 4. Comparison of three different electrostatic transducers. (a) Parallel plate transducers at beam ends. The transducers have areas $A = WH$ and gaps d. (b) Internal transducer in the beam center. The transducer has area $A = WH$ and a gap d (transducer edges are at $-d/2$ and $d/2$). (c) Poisson's effect transducer on top of the beam. As the transducer is actuated in the thickness direction, it transforms motion to lateral deformation due to the Poisson's effect. The transducer has area $A = WL$ and thickness h.

and the excitation force on the left side of the infinitesimal beam element is $f_e|_{\frac{L}{2}-\Delta x} = 0$. Thus, the gradient of the force is:

$$\frac{\partial f_e}{\partial x} = \lim_{\Delta x \to 0} \frac{f_e|_{\frac{L}{2}} - f_e|_{\frac{L}{2}-\Delta x}}{\Delta x} = \frac{\epsilon_p WH}{d^2} V_{\mathrm{dc}} v \delta(x - L/2), \tag{15}$$

where δ is the delta-function. At the left end, the force has the same magnitude but opposite direction. Thus, the total force gradient acting on the beam is:

$$\frac{\partial f_e}{\partial x} = \frac{\epsilon_p WH}{d^2} V_{\mathrm{dc}} v (\delta(x - L/2) - \delta(x + L/2)). \tag{16}$$

Alternative formulation for the force f_e is obtained by noting that the electrostatic pulling force acting on the beam ends results in tensile force (stress) inside the beam given by:

$$f_e = \frac{\epsilon_p WH}{d^2} V_{\mathrm{dc}} v, \quad x \in [-L/2, L/2], \tag{17}$$

where (16) and (17) give mathematically equal results. This is similar to the piezoelectric transducers in which the coupling may be modeled as distributed stress acting in the transducer volume or lumped force at the transducer edge [12]. Substituting (16) or (17) into (6) gives:

$$F_p = \eta_p v, \tag{18}$$

where:

$$\eta_p = 2\frac{\epsilon_p W H}{d^2} V_{\mathrm{dc}}. \tag{19}$$

As expected, the transduction factors given by (19) and (11) are the same. The motional current is:

$$i_m = \frac{\partial C}{\partial t} V_{\mathrm{dc}} = 2\frac{\partial}{\partial t}\left(\frac{\epsilon_p W H}{d - X}\right) V_{\mathrm{dc}} \approx \eta_p \dot{X}. \tag{20}$$

B. Internal Transducer

Fig. 4(b) shows a beam with an internal actuator placed at the nodal point [4]. For simplicity, we assume that the actuator material has the same density and Young's modulus as the beam and, therefore, does not affect the resonant frequency and mode shape. The capacitive force acting in the transducer area is:

$$f_e = -\frac{\epsilon_i W H}{d^2} V_{\mathrm{dc}} v, \quad x \in [-d/2, d/2], \tag{21}$$

where ϵ_i is the permittivity for the internal transducer material. Substituting (21) into (6) gives:

$$F_i = \eta_i v, \tag{22}$$

where:

$$\eta_i = -2\sin\left(\frac{kd}{2}\right)\frac{\epsilon_i W H}{d^2} V_{\mathrm{dc}} \approx -\frac{\pi d}{L}\frac{\epsilon_i W H}{d^2} V_{\mathrm{dc}}. \tag{23}$$

The approximation is valid for $\pi d/L \ll 1$. In writing (23), the terms have been grouped to facilitate comparison to the parallel plate transduction coefficient given by (19). The motional current is:

$$i_m = \frac{\partial C}{\partial t} V_{\mathrm{dc}} = \frac{\partial}{\partial t}\left(\frac{\epsilon_i W H}{d + 2X\sin(kd/2)}\right) V_{\mathrm{dc}} \approx \eta_i \dot{X}. \tag{24}$$

C. Poisson's Effect Transducer

Fig. 4(c) shows a beam with a transducer on the top surface [5]. As the transducer is a thin film on top of the resonator, it may deform in the z direction without external constraints, but the lateral movement is constrained by the beam.

The main force generated by the electric field over the transducer is in the thickness direction; but, due to the Poisson's effect, the thin film also will have lateral stresses. This lateral film stress will actuate the beam in the length direction. For simplicity, we assume that the actuator does not change the beam resonant frequency or the mode shape; the actuator material is assumed to have the same Young's modulus and density as the beam, or to be sufficiently thin.

The capacitive force generates stress within the thin film in the z direction given by:

$$T_z = \frac{\epsilon_\nu}{h^2} V_{\mathrm{dc}} v, \tag{25}$$

where h is the transducer thickness. Due to the Poisson's effect, the stress in the z direction generates stress also in the x and y directions. The upper limit for the stress in the film in the x direction:

$$T_x = \frac{\nu}{1-\nu} T_z, \tag{26}$$

is obtained if the film is firmly anchored to the resonator and cannot freely deform laterally ($S_x = S_y = 0$). This is a good approximation for a flexible or thin film. If lateral deformations were allowed, the stress in the x direction would be lowered. The validity of the approximation $S_x = S_y = 0$ is discussed in Section V in which the analytical expressions are compared to the finite-element results.

The resulting force that actuates the beam can be obtained by multiplying the stress in the film by the film cross-sectional area $A = Wh$ leading to:

$$f_e = T_x W h, \quad x \in [-L/2, L/2]. \tag{27}$$

Substituting (27) into (6) gives:

$$F_\nu = \eta_\nu v, \tag{28}$$

where:

$$\eta_\nu = 2\frac{\nu}{1-\nu}\frac{h}{H}\frac{\epsilon_\nu W H}{h^2} V_{\mathrm{dc}}. \tag{29}$$

For given vibration amplitude, the strain in the x direction is $S_x = (\partial u_x/\partial x) = Xk\cos(kx)$. As the film can deform freely in the z direction, the strain S_x also will generate strain in the z direction. Assuming no y-displacement gives the upper limit for the transducer strain in the z direction:

$$S_z = -\frac{\nu}{1-\nu} S_x. \tag{30}$$

The change in capacitance per unit length dx is:

$$\frac{\partial \mathrm{d}C}{\partial t} = \frac{\partial}{\partial t}\left(\frac{\epsilon_\nu W \mathrm{d}x}{h}\right) = -\frac{\epsilon_\nu W \mathrm{d}x}{h}\frac{\dot{h}}{h}. \tag{31}$$

Recognizing:

$$\frac{\dot{h}}{h} = \dot{S}_z = -\frac{\nu}{1-\nu}\dot{S}_x = -\frac{\nu}{1-\nu}\dot{X}k\cos(kx), \tag{32}$$

and integrating over the beam length gives the motional current:

$$i_m = \frac{\partial C}{\partial t} V_{\mathrm{dc}} = \int_{-L/2}^{L/2} \frac{\epsilon_\nu W}{h}\dot{S}_x \mathrm{d}x = \eta_\nu \dot{X}. \tag{33}$$

In deriving the transduction coefficient, the ratio $\nu/(1-\nu)$ was based on simplified assumptions of lateral deformations and gives the upper limit for the coupling coefficient. More detailed considerations and/or finite-element modeling may be required if accurate geometrical dependency is needed, especially if the film cannot be considered thin. However, as shown by finite-element method (FEM) analysis in Section V, the ratio $\nu/(1-\nu)$ is sufficiently accurate for estimating the magnitude and upper limit of the coupling.

TABLE I
Ratio of Transduction Coefficients.

Ratio	η_i/η_p	η_ν/η_p
Expression	$\frac{\pi}{2}\frac{d}{L}\frac{\epsilon_i}{\epsilon_p}$	$\frac{\nu}{(1-\nu)}\frac{d^2}{hH}\frac{\epsilon_\nu}{\epsilon_p}$
Analytical	0.0082	0.067
FEM	0.0082	0.046

V. Comparison of Transducers and FEM Verification

In Section IV, three different coupling methods were considered; and it was found that one parameter, the electrostatic transduction factor, fully characterizes the transducers. Table I shows a comparison of the electrostatic transduction coefficients. As a specific example, a beam resonator with $L = 300$ μm, $H = 10$ μm, $h = d = 200$ nm, $\epsilon_p = \epsilon_0$, $\epsilon_i = \epsilon_\nu = 7.8\epsilon_0$ corresponding to silicon nitride, and $\nu = 0.3$ is considered.

The analytical results are compared to numerical finite-element (FEM) results obtained with ANSYS software[2]. The frequency-domain ("harmonic") 3-D FEM model is based on isotropic "solid45" elements, and a total of 5436 nodes were used in the simulations. Full harmonic-response solution was used to accurately simulate the vibration at the resonance. The fringing-field effects were ignored in the simulations as they can be assumed insignificant for the narrow-gap devices. To verify the accuracy, the simulations also were run with an increased node count of 36421 (volume of the elements reduced by a factor of eight). The difference in the results was less than 1%, indicating a good numerical convergence.

For the ratio of the internal and parallel plate transducers, one obtains $\eta_i/\eta_p = 0.0082$ both analytically and with FEM. The small ratio is due to the conventional parallel plate transducer affecting the optimal location of maximum resonator displacement; the internal transducer is located in the small displacement region. This unfavorable ratio may be improved by using several internal transducers in parallel and/or higher permittivity transducer material such as titanium dioxide with $\epsilon \sim 85\epsilon_0$. However, it appears that the internal transducer does not offer a clear advantage over the parallel plate transducer.

For the Poisson's effect, one obtains the analytical and FEM results of $\eta_\nu/\eta_p = 0.067$ and 0.046, respectively, for the force η in (28). The FEM result is about 30% smaller than the analytical result as the ratio $\nu/(1-\nu)$ gives the upper limit for the coupling. Incidentally, if $\nu/(1-\nu)$ is changed to ν, the agreement is within 3% for the force coupling coefficient. The simulated current coupling coefficient in (33) was slightly different (0.056). The differing values of the coupling coefficients for the force and current indicate that the 1-D model is not sufficient for accurate design and 3-D simulation or model is needed. However, the simple 1-D model is an excellent order-of-magnitude estimate for the coupling coefficients.

The Poisson's effect coupling gives equal performance as the parallel plate transducer if the transducer height is $h = 13$ nm or roughly 15 times smaller than the parallel plate transducer gap d with the associated decrease in the transducer linearity. We note that the Poisson's effect transducer may be easier to manufacture than the parallel plate transducer of equal performance as it is relatively easy to deposit a thin film in comparison to defining submicron vertical gaps. However, the asymmetric excitation affecting only the top of the beam may lead to excitation of flexural modes. Also, any instability in the transducer or transducer-resonator interface leads to degradation of the long-term resonator stability.

We note that the performance of the conventional parallel plate transducer may be improved by the introduction of higher permittivity dielectric in the transducer gap [7]. The full analysis of solid-dielectric transducer placed in the location of maximum displacement is, however, beyond the scope of this paper as this would require modeling the counter electrode motion and the resulting losses in efficiency.

[2]ANSYS, Inc., www.ansys.com.

VI. Conclusions

The electrostatic transduction was considered for a specific example of a micromechanical beam resonator. The conventional parallel plate transducer is seen to offer relatively good performance as the electrostatic force affects the optimal location of maximum displacement. The internal transducer with solid dielectric is seen to offer poor performance due to the force being located in the small-displacement region. The Poisson's effect transducer offers performance comparable to the parallel plate transducer with gap d provided that the film thickness is $h \approx \epsilon_\nu d^2/\epsilon_p H$. Thus, for typical values, the film thickness should be a factor of 10 smaller than the gap in the parallel plate transducer to reach similar performance.

References

[1] V. Kaajakari, T. Mattila, A. Oja, J. Kiihamäki, and H. Seppä, "Square-extensional mode single-crystal silicon micromechanical resonator for low phase noise oscillator applications," *IEEE Electron. Device Lett.*, vol. 25, no. 4, pp. 173–175, Apr. 2004.

[2] J. Wang, Z. Ren, and C. T.-C. Nguyen, "1.156-GHz self-aligned vibrating micromechanical disk resonator," *IEEE Trans. Ultrason., Ferroelect., Freq. Contr.*, vol. 51, no. 12, pp. 1607–1628, Dec. 2004.

[3] A. T. Alastalo and V. Kaajakari, "Third-order intermodulation in microelectromechanical filters coupled with capacitive transducers," *J. Microelectromech. Syst.*, vol. 15, no. 1, pp. 141–148, Feb. 2005.

[4] S. A. Bhave and R. T. Howe, "Internal electrostatic transduction for bulk-mode MEMS resonators," in *Proc. Solid State Sensor, Actuator Microsyst. Workshop*, 2004, pp. 59–60.

[5] S. A. Bhave and R. T. Howe, "Silicon nitride-on-silicon bar resonator using internal electrostatic transduction," in *Proc. 13th Int. Conf. Solid-State Sens. Actuators*, 2005, pp. 2139–2142.

[6] A. Alastalo, T. Mattila, and H. Seppä, "Analysis of a MEMS transmission line," *IEEE Trans. Microwave Theory Tech.*, vol. 51, no. 8, pp. 1977–1981, Aug. 2003.

[7] Y.-W. Lin, S.-S. Li, Z. Ren, and C. T.-C. Nguyen, "Vibrating micromechanical resonators with solid dielectric capacitive transducer gaps," in *Proc. IEEE Int. Freq. Contr. Symp.*, 2005, pp. 128–134.

[8] T. Mattila, J. Kiihamäki, T. Lamminmäki, O. Jaakkola, P. Rantakari, A. Oja, H. Seppä, H. Kattelus, and I. Tittonen, "12 MHz micromechanical bulk acoustic mode oscillator," *Sens. Actuators A*, vol. 101, no. 1–2, pp. 1–9, Sep. 2002.

[9] M. Alonso and E. J. Finn, *Fundamental University Physics*. 2nd ed. vol. 2, Reading, MA: Addison-Wesley, 1983.

[10] K. F. Graff, *Wave Motion in Elastic Solids*. New York: Dover, 1975.

[11] B. A. Auld, *Acoustic Fields and Waves in Solids*. 2nd ed. Malabar, FL: Krieger, 1990.

[12] R. Holland and E. P. EerNisse, *Design of Resonant Piezoelectric Devices*. Cambridge, MA: MIT, 1969.